Supporting Information

Chakraborty et al. 10.1073/pnas.1410440111

SI Materials and Methods

Sample Purification and Blank Correction. Several sample purifications steps have been adopted in processing each sample: (*i*) The photolysis product of each run was cryogenically separated from moisture by using a −10 °C ethanol shush before pyrolysis, and (*ii*) after pyrolysis, the product N_2 was cryogenically separated from other pyrolysis products (e.g., H_2O). After inserting the pure N_2 in to the isotope-ratio mass spectrometer, a scan was performed to check for impurities, if any. Special care was taken to identify traces of CO present in the sample as being the same mass, which could interfere with the measurement. In the mass scan, no impurities are found for any of the samples.

Several blank experiments are performed, following all of the steps in the experiment starting from gas-mixture flow in the reaction chamber through pyrolysis of the product [excluding vacuum UV (VUV) photons] over a 3-y period. A capacitance manometer (Baratron 626) with a full scale of 10 Torr was used to measure the N_2 yield. In the experimental configuration (considering the volume of the vacuum line), the lower limit of sample size, which the manometer can reliably measure, is 0.01 μmol (with a SD of 5% of the reading). All of our blank samples are at that limit, and we adopted a value of 0.01 μmol for the blank correction. The average value of isotope ratio measurement is $\delta^{15}N = 18.3‰ \pm 0.6‰$ ($n = 5$). The SD of individual sample runs in the mass spectrometer is much lower, 0.06‰. This value was subtracted from each measured $\delta^{15}N$ number by isotope mass balance by the following formula:

$$\delta^{15}N_{actual} = \left[\left(\delta^{15}N_{measured} * A_{measured}\right) - \left(\delta^{15}N_{blank} * A_{blank}\right)\right] / A_{actual},$$

where "A"s are the amounts of different components as indicated by the subscripts.

Ionization of Gases. It is important to note that photoionization of N_2 will not play a role because the ionization energy of N_2, H_2, and H are 14.534, 15.42, and 13.6 eV, respectively, and are greater than the energy used in these experiments. However, the ionization energy of NH_3 is 10.2 eV and may suffer photoionization at the wavelengths used in these experiments (1) and may introduce additional isotope effects. The isotope effect in photoionization of N_2 (2) is negligible compared with photodissociation fractionation presented here and, therefore, it can be assumed that the photoionization fractionation of NH_3 is negligible.

Use of Low H_2/N_2 Ratio. The H_2 to N_2 ratio in the solar nebula is much higher compared with that of the experiments, as higher H_2/N_2 ratio would have yielded much lower NH_3 within the experimental time scale. The purpose of the present study is to establish that the N_2 photodissociation process is a highly fractionating N-isotopic process and photolytic products may be effectively be trapped in NH_3. For the solar nebula, this could be accommodated in a few million years' VUV irradiation time.

Self-Shielding: Computational Methodology. ***Spectrum.*** To accurately compute the photolysis processes inside the reaction chamber, including temperature and pressure effects, a rotationally resolved spectrum for each of the isotopomers was computed (Fig. S1). In the first step, the vibrational spectrum of the N_2 molecule in the range ∼100,000–120,000 cm^{-1} (100–83.3 nm), including all three optically accessible excited electronic states of a given symmetry, was computed. The oscillator strength of each line was normalized to fit the experimental value $f = 0.043$ of the $b^1\Pi(v = 3)$ level (3).

A rotational line spectrum was superposed on the vibrational spectrum. The total cross section of each vibronic line is the sum of cross sections of all associated rotational lines. The shape of each rotational line is that of a Doppler line shape (4):

$$k(\nu) = k_0 \frac{2\sqrt{\ln 2}}{\pi(\Delta\nu)} \exp\left[-4 \ln 2 \frac{(\nu - \nu_0)^2}{(\Delta\nu)^2}\right]. \qquad \textbf{[S1]}$$

The line broadening used here is a sum of the Doppler broadening and the natural broadening $\Delta\nu = \Delta\nu_{dop} + \Delta\nu_{nat}$. The value of the natural broadening $\Delta\nu_{nat}$ (related to the predissociation lifetime) was taken to be the experimental value as presented in the supporting information of ref. 5. Where an experimental value of the width was absent, a value of 0.2 cm^{-1} was assigned—an average value for the rotational width in this range of energies. In cases in which only one isotope's rotational line width is known, the other two isotopes' rotational widths were set to the same value. In cases where only the widths for the isotopes $^{14}N_2$ and $^{15}N_2$ are known, the average value of the two was taken for $^{14}N^{15}N$.

A source of temperature and mass dependence is the Doppler broadening, taken here as $\Delta\nu_{dop} = (2/c)\sqrt{2R \ln 2}\nu_0\sqrt{T/M}$ (4). Generally the Doppler broadening in this experiment was about 0.01 cm^{-1}—smaller than the natural broadening. The relative line strength of each rotational level within each rotational packet is affected by three factors: Boltzmann statistics, nuclear spin statistics, and Hoenl–London (HL) factors. The Boltzmann distribution for the rotational levels is (4):

$$I_{abs} \propto (2J + 1)e^{-E_J/k_B T},$$

where J is the rotational state, E_J the rotational energy, T is the temperature, and k_B is the Boltzmann constant. The moment of inertia is isotope dependent and also electronic state dependent because the equilibrium distance differs for each electronic state. The values of the equilibrium distances were taken from ref. 6. The second factor that affects the relative intensity of each rotational line is spin statistics. The total wave function of the system (4) $\Psi_{tot} = \Psi_{electron}\Psi_{rotation}\Psi_{nuclear\ spin}$ must be antisymmetric. The rotationally even levels $J = 0, 2, 4\ldots$ are symmetric, while the odd levels are antisymmetric. The electronic wave function can be symmetric or antisymmetric. The nuclear wave function symmetry depends on the overall nuclear spin I, which is 1 for the ^{14}N atom and 1/2 for the ^{15}N atom. The total spin of the molecule is given by $I = (2I_a+1)(2I_b+1)$, and there are a total of $(2I+1)^2$ nuclear spin states: $(2I+1)(I+1)$ states are symmetric and $(2I+1)I$ states are antisymmetric. For a Σ-state excitation, the relative weights, (states of even J):(states of odd J), are found to be 2:1 for $^{14}N_2$, 1:1 for $^{14}N^{15}N$, and 3:1 for $^{15}N_2$. The opposite weights are obtained for a Π-state excitation. The third element in determining the rotational distribution is given by the HL factors (7). These factors define how the intensities of the rotational line are distributed between the rotational branches R, P, and Q. For a Σ→Π transition, all three branches exist, but for a Σ→Σ transition, only the R and P branches exist due to selection rules (8). The HL factors used here are taken from ref. 8.

Over wide regions of frequency, the rotational spectrum has the band structure and the band envelope shifts with temperature as

expected. The absorption spectrum also shifts with the isotopic composition in the manner expected from the familiar mass dependence of the vibrational and rotational constants. The situation is quite different in those regions of the spectrum where extensive electronic state mixing occurs, as shown in Fig. S3 for the location about 90 nm.

In addition to nitrogen, H_2 comprises 50% of the gas in the chamber. Although it has much weaker absorption lines in the spectral range of interest, for reasons of accuracy, we included its cross section in the simulation. We obtained the rotational spectrum of H_2 from the MOLAT project (9) database (http://molat.obspm.fr/index.php?page=accueil.php).

We simulated the absorption of the three isotopomers for the different conditions of the experiment. Since the radiative lifetimes for all states in the energy range of 100,000–120,000 cm^{-1} are much longer (on the order of nanosecond) than the predissociation lifetimes (hundreds of picoseconds or less), we invoked the assumption that the quantum yield of dissociation is about unity. This means that all excited states will eventually dissociate. The absorption spectrum is thus equal to the predissociation yield.

Shielding. The absorption of each isotopomer was calculated using the Beer–Lambert law, and the result was summed over the three isotopes to give the light intensity at the wavelength λ at a distance l along the length of the chamber:

$$I_\lambda(l) = I_\lambda^{ALS} \exp\left(-\sum_{isotopes} \sigma_\lambda^{iso} l \cdot c^{iso}\right). \quad \textbf{[S2]}$$

I_λ^{ALS} is the Advanced Light Source synchrotron (ALS) beam intensity at a particular wavelength (λ) at the entrance to the chamber, σ^{iso} is the isotopologues specific cross section, and c^{iso} is the concentration of the isotopologues of N_2 (the abundances of $^{14}N_2$, ^{14}N ^{15}N, and $^{15}N_2$ are 0.99273325, 0.0072535, and 0.00001325, respectively). At the given wavelength, a particular isotopologue absorbs as given by

$$J^{iso}(l) = \int I_\lambda(l)\sigma_\lambda^{iso} d\lambda. \quad \textbf{[S3]}$$

By our assumption of a quantum yield of dissociation of unity, Eq. **S4** also gives the yield of dissociation. Summing over the length of the chamber gives

$$J^{iso} = \int_0^{l\max} J^{iso}(l) dl. \quad \textbf{[S4]}$$

The isotopic fractionation was computed by the conventional form:

$$\delta^{15}N \equiv 1{,}000\left(\frac{(^{15}N/^{14}N)_{sample}}{(^{15}N/^{14}N)_{standard}} - 1\right)$$
$$= 1{,}000\left(\frac{\left(\frac{J^{1415}\cdot c^{1415}}{J^{1414}\cdot c^{1414}}\right)_{sample}}{(c^{1415}/c^{1414})_{standard}} - 1\right) = 1{,}000\left(\frac{J^{1415}}{J^{1414}} - 1\right). \quad \textbf{[S5]}$$

The standard concentrations are for air at atmospheric level. The formula (in permil) neglects the contribution of the $^{15}N_2$ molecules to the total number of ^{15}N atoms in the chamber; this is reasonable due to the very low $^{15}N_2$ concentration. The isotopic fractionation $\delta^{15}N$ was computed as a function of the central frequency of the ALS beam profile, for the entire frequency range 100,000–120,000 cm^{-1} and for different densities and temperatures.

Nitrogen Photochemistry: Additional Discussion. The single-photon electronic spectroscopy of N_2 has been very extensively studied both experimentally and theoretically. It has also been compared with its isoelectronic counterpart, CO (10). Like CO, N_2 absorbs photons through discrete lines in the VUV region and dissociates via predissociative pathways. The absorption bands of N_2 can be divided into two regimes: above and below 100 nm. Above 100 nm, there are only a few absorption bands, and below 100 nm, there are several. There are several similar molecular absorption properties of N_2 and CO. For example, there are several bound excited states of Σ and Π symmetry and two Rydberg and one valence excited state for each symmetry. The properties of the Rydberg states (force constant and equilibrium distance) are comparable to those of the ground state, and the low-lying vibrational rational states for each Rydberg electronic state are within the Franck–Condon region and consequently exhibit an intense absorption transition. The potential energy curves for the valence excited states are shallower, and it is the higher vibrational states that are within the Franck–Condon primary absorption region (5). As a consequence of mixing of Rydberg and valence states of either symmetry (11–19), perturbations are common and are observed as irregularities of the spectrum. These perturbations and predissociation have been very well studied for N_2; however, for CO, they are not as yet completely quantified (10). Apart from direct predissociation, accidental predissociation is observed for both molecular systems. The predissociation of N_2 is indirect and occurs primarily due to the mixing (through spin–orbit coupling) of the bound, optically accessible, valence state $b^1\Pi$ to the bound $C^3\Pi$ triplet state that predissociates to the $C'^3\Pi$ state (20–22). An analogous indirect predissociation occurs for the $E^1\Pi$ (bound) state of CO, when it mixes with the $k^3\Pi$ state, which predissociates through a $^3\Pi$ repulsive surface (18, 19, 23).

A detailed quantum mechanical calculation of the wavelength dependence for the photoexcitation process has been recently presented by our group (5). In this computation, special attention has been paid to those regions in the spectrum where the perturbations are particularly sensitive to the isotopic composition of the molecule. Typical results are shown in Fig. S2.

As discussed in the *Discussion, Perturbation-Governed Isotope Effect*, we propose that isotope effect in N_2 could be a result of the extensive state mixing that occurs in localized regions of the spectrum as, for example, the b′-c′ mixing shown at about 144,000–147,000 cm^{-1} in Fig. S1. In particular, a very extensive state mixing occurs at 90 nm (111,111 cm^{-1}) and is shown including the rotational structure.

Under the given experimental conditions, the isotopic fractionation is dominated by shielding effects. A first illustration of this is how the isotopic fractionation varies with temperature (Fig. S3), other variables being the same. Examination of the details verifies that the trend shown in Fig. S3*A* is the broadening of the rotational bands with increasing temperature. As its spectrum broadens, the common isotopomer $^2N_{14}$ is better able to shield $^{14}N^{15}N$ and thereby decrease the fractionation. The trend is as observed experimentally; see Table 1. However, except at the region around 90 nm, we compute less shielding than is needed to account for the experimental results. To reproduce the experiment at other wavelengths, we need to include rotational bands that are about 4 cm^{-1} broad. We do not have an explanation for such a broadening. To test for the possibility that the excessive shielding is a pressure effect, we repeated the computations as a function of pressure (Fig. S3*B*). The results are rather nonmonotonic. The fractionation is low for 0.001 Torr, increases for 0.01 Torr and 0.1 Torr, and drops down again for 1 Torr and 10 Torr. The physical explanation is again shielding,

but mutual shielding plays a larger role than self-shielding at higher pressures. For low pressure, the self-shielding is weak since the effect originates from the absorbance of the abundant isotopomer. An increase in pressure is accompanied by an increase in self-shielding and relatively higher absorption (and predissociation) of the rare isotopes in comparison with the initial isotopic composition. This effect saturates and then drops off because at the higher pressures, the rarer isotopomer is dense enough to undergo self-shielding of its own accord. As a result, there is no longer any isotopic preference in the photoexcitation process.

1. Xia TJ, Chien TS, Wu CYR, Judge DL (1991) Photoabsorption and photoionization cross sections of NH_3, PH_3, H_2S, C_2H_2, and C_2H_4 in the VUV region. *J Quant Spectrosc Radiat Transfer* 45(2):77–91.
2. Philip C, et al. (2011) Measurements of isotope effects in the photoionization of N_2 and implications for Titan's atmosphere. *Astrophys J Lett* 728(2):L32.
3. Stark G, Huber KP, Yoshino K, Smith PL, Ito K (2005) Oscillator strength and linewidth measurements of dipole-allowed transitions in $^{14}N_2$ between 93.5 and 99.5 nm. *J Chem Phys* 123(21):214303.
4. Steinfeld JI (1985) *Molecules and Radiation* (MIT Press, Cambridge, MA), 2nd Ed.
5. Muskatel BH, Remacle F, Thiemens MH, Levine RD (2011) On the strong and selective isotope effect in the UV excitation of N_2 with implications toward the nebula and Martian atmosphere. *Proc Natl Acad Sci USA* 108(15):6020–6025.
6. Spelsberg D, Meyer W (2001) Dipole-allowed excited states of N_2: Potential energy curves, vibrational analysis, and absorption intensities. *J Chem Phys* 115(14): 6438–6449.
7. Hoenl H, London F (1925) *Z Phys* 33:803.
8. Herzberg G (1989) *Molecular Spectra and Molecular Structure: Spectra of Diatomic Molecules* (Krieger, Malabar, FL), 2nd Ed.
9. Abgrall H, Roueff E (2006) Theoretical calculations of excited rovibrational levels of HD. Term values and transition probabilities of VUV electronic bands. *Astron Astrophys* 445(1):361–372.
10. Lefebvre-Brion H, Lewis BR (2007) Comparison between predissociation mechanisms in two isoelectronic molecules: CO and N_2. *Mol Phys* 105(11-12):1625–1630.
11. Huber KP, Chan M-C, Stark G, Ito K, Matsui T (2009) N_2 band oscillator strengths at near-threshold energies. *J Chem Phys* 131(8):084301.
12. Huber KP, Jungen C (1990) High-resolution jet absorption study of nitrogen near 800 Å. *J Chem Phys* 92(2):850–861.
13. Huber KP, Jungen C, Yoshino K, Ito K, Stark G (1994) The f Rydberg series in the absorption spectrum of N_2. *J Chem Phys* 100(11):7957–7972.
14. Lefebvre-Brion H, Liebermann HP, Vázquez GJ (2010) An interpretation of the anomalous $^1\Pi$ vibronic structure in the far-UV spectrum of CO. *J Chem Phys* 132(2): 024311.
15. Mellinger A, Vidal CR, Jungen C (1996) Laser-reduced fluorescence study of the carbon monoxide nd triplet Rydberg series: Experimental results and multichannel quantum defect analysis. *J Chem Phys* 104(22):8913–8921.
16. Baker J, Launay F (2005) Identification and analysis of the perturbed $c^3\Pi(v = 1) - X^1\Sigma^+$ and $k^3\Pi(v = 5) - X^1\Sigma^+$ absorption bands of carbon monoxide. *J Chem Phys* 123(23): 234302.
17. Eikema KSE, Hogervorst W, Ubachs W (1994) On the determination of a heterogeneous vs a homogeneous perturbation in the spectrum of a diatomic molecule: The $K1\Sigma^+$, $v = 0$ state of $^{13}C^{18}O$. *J Mol Spectrosc* 163(1):19–26.
18. Ubachs W, Velchev I, Cacciani P (2000) Predissociation in the $E^1\Pi$, v = 1 state of the six natural isotopomers of CO. *J Chem Phys* 113(2):547–560.
19. Cacciani P, Hogervorst W, Ubachs W (1995) Accidental predissociation phenomena in the $E^1\Pi$, v=0 and v=1 states of $^{12}C^{16}O$ and $^{13}C^{16}O$. *J Chem Phys* 102(21):8308–8320.
20. Lefebvre-Brion H, Field RW (2004) *The Spectra and Dynamics of Diatomic Molecules* (Elsevier, New York), 2nd Ed.
21. Lewis BR, Gibson ST, Zhang W, Lefebvre-Brion H, Robbe J-M (2005) Predissociation mechanism for the lowest $^1\Pi_u$ states of N_2. *J Chem Phys* 122(14):144302.
22. Muskatel BH, Remacle F, Levine RD (2012) Ultrafast predissociation mechanism of the $^1\Pi_u$ states of $^{14}N_2$ and its isotopomers upon attosecond excitation from the ground state. *J Phys Chem A* 116(46):11311–11318.
23. Simmons JD, Tilford SG (1974) Evidence for an accidental predissociation of CO. *J Mol Spectrosc* 49(1):167–168.

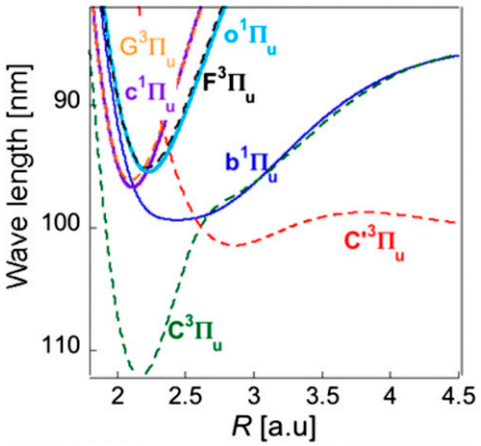

Fig. S1. Schematic potential energy diagram of N_2. Lowest dipole allowed from the ground state diabatic $^1\Pi_u$ states (solid lines) adapted from ref. 6. The pi and sigma states are dipole allowed for different polarizations of the light source. $^3\prod_u$ states are shown by dashed lines. The reference energy is of the $X^1\Sigma_g(\nu=0)$ state. Predissociation occurs to the continuum of the repulsive $C'^3\Pi_u$ state.

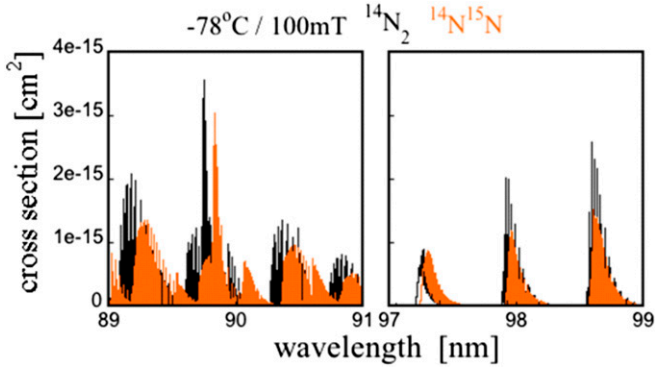

Fig. S2. Comparison of rovibrational spectrum of $^{14}N_2$ and $^{14}N^{15}N$ at two different spectral regions. The region around 90 nm is unique, showing strong electronic state mixing leading to massive N-isotopic fractionation, whereas weak state mixing (with well resolved vibronic bands) is seen at around 98 nm and the isotopic fractionation is relatively smaller. The details of this computation are given in *SI Materials and Methods, Self-Shielding: Computational Methodology*.

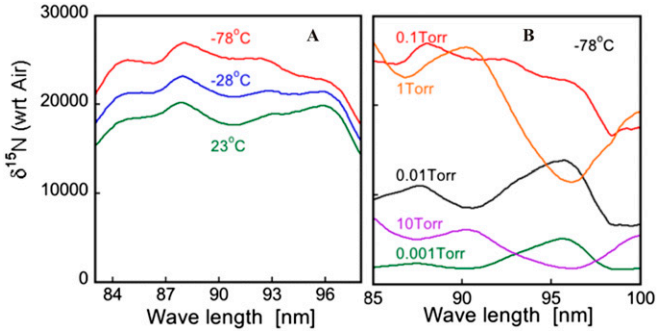

Fig. S3. Temperature- and pressure-dependent enrichment profiles of ^{15}N [with respect to (wrt) air composition] using the photoabsorption cross-section data as shown in Fig. S3. (*A*) Isotopic enrichment decreases with increasing temperature, where pressure is kept constant at 0.1 torr in the simulation. (*B*) Pressure-dependent isotopic enrichment profiles at a fixed temperature of −78 °C.

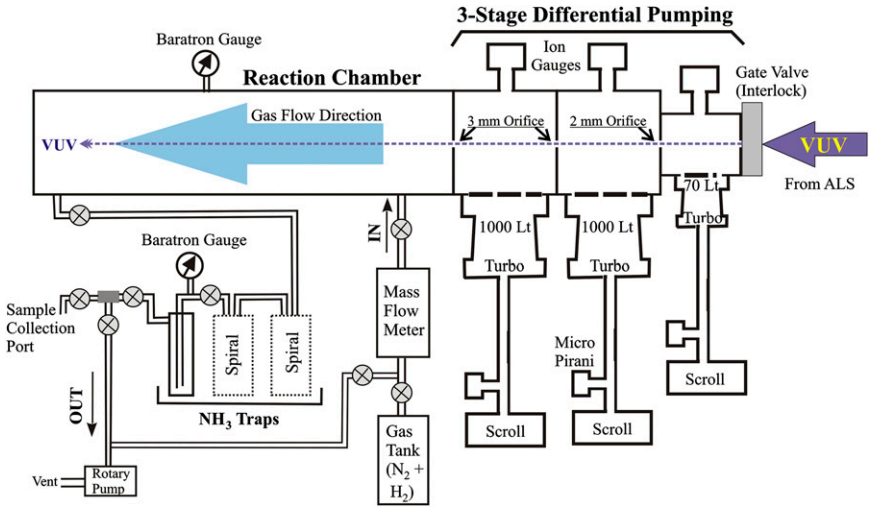

Fig. S4. Schematic diagram of the differential pumping system used for photodissociation of N_2 at the Advanced Light Source (ALS) synchrotron.